Journal of Mineralogical and Petrological Sciences, Volume 116, page 293–308, 2021

Geochronology and geochemistry of granitoids from the Mongolian Altai

Dolzodmaa BOLDBAATAR[*], Yasuhito OSANAI[**], Nobuhiko NAKANO[**], Tatsuro ADACHI[**], Jargalan SEREENEN[***], Ippei KITANO[**,†] and Kundyz SYERYEKKHAAN[‡]

[*]*Graduate school of Integrated Sciences for Global Society, Kyushu University, Fukuoka 819-0395, Japan*
[**]*Division of Earth Sciences, Faculty of Social and Cultural Studies, Kyushu University, Fukuoka 819-0395, Japan*
[***]*Department of Mineral Exploration, Mongolian University of Science and Technology, Ulaanbaatar 14191, Mongolia*
[†]*Tochigi Prefectural Museum, Utsunomiya 320-0865, Japan*
[‡]*Golden Hill LLC, Ulaanbaatar 14182, Mongolia*

Granitoid magmatism is widespread in the Mongolian Altai, and it provides critical information to understand the crustal formation, evolution, and growth. This study reports newly investigated petrography, whole-rock geochemistry, and zircon U-Pb geochronology of granites and quartz syenites emplaced in the Mongolian Altai to investigate their sources and petrogenesis. Our results allow that granitoids, five petrological groups, and four geochronological stages from this study provide new information to understand the crustal formation and evolution of the Mongolian Altai. Geochemically, the group-I (Bt-Ms granite) and -II (Crd-Bt granite) have high-K calc-alkaline and peraluminous affinity, whereas group-III (Hbl-Bt granite) has calc-alkaline and metaluminous affinity. Group-IV (Bt quartz syenite) and -V (Kfs-porphyritic granite) show shoshonitic- to high-K calc-alkaline and metaluminous characteristics. The zircon U-Pb dating constraints the Devonian magmatic ages of 387–361 Ma for group-I, 369–353 Ma for group-II, and 366–356 Ma for group-III granites, whereas ~ 315 Ma for group-IV quartz syenite and 208–200 Ma for group-V granite. Groups-I and -II peraluminous granites have high-Th/Nb, and low-Ba/Th reflecting sources might be derived from sedimentary rocks, whereas group-III metaluminous granite has low-Th/Nb and high-Ba/Th reflecting a source that might be derived from gabbroic crustal material. Groups-I and -II peraluminous granites have similar geochemical characteristics, but their emplacement ages are different, which suggests they were formed from different magmas. Group-II peraluminous and group-III metaluminous granites were contemporaneous, and their Rb/Ba versus Rb/Sr correlation define a linear trend of the magma mixing process. It demonstrates that group-III metaluminous magma would carry heat to the crust, inducing partial melting of sedimentary rocks to produce group-II peraluminous granite. Finally, geochemical and geochronological data of groups-I, -II, and -III granites demonstrate that they were formed during the main orogenic activity in the Mongolian Altai, which is consistent with the timing of the main metamorphic event at Late Devonian to Early Carboniferous. Subordinated group-IV quartz syenite and group-V granite were probably formed in extensional to post-collisional environments after main orogenic activity in the Mongolian Altai.

Keywords: Zircon U-Pb age, Geochemistry, Magma evolution, Mongolian Altai granitoids

INTRODUCTION

The continental crust consists of highly diverse lithologies (virtually every rock type known on Earth) that yield an average intermediate or 'andesitic' bulk composition (Taylor and McLennan, 1995 and references therein) and contains the oldest rocks and minerals yet observed on the Earth (e.g., Jahn et al., 2000; Rudnick, 2003). Granitoid is one of the most common constituent rocks in the continental crust, providing critical information to understand the crustal formation, evolution, and growth since they were produced at different evolutionary stages, under different tectonic regimes, and different magmatic sources (e.g., Barbarin, 1999; Jahn et al., 2000; Arndt,

doi:10.2465/jmps.210830
D. Boldbaatar, boldbaatar.dolzodmaa.584@s.kyushu-u.ac.jp Corresponding author
Y. Osanai, osanai@scs.kyushu-u.ac.jp

2013). This paper focuses on the formation and evolution of the Mongolian Altai granitoids in the Central Asian Orogenic Belt (CAOB). The CAOB is geologically situated among four cratons (the Baltica, Siberia, North China, and Tarim cratons; Fig. 1) and characterized by the vast distribution of Paleozoic and Mesozoic granitic intrusions as well as basaltic to rhyolitic volcanic activities (Jahn et al., 2000). The CAOB is widely considered as a major site of juvenile crustal growth (e.g., Jahn et al., 2000; Badarch et al., 2002; Kozakov et al., 2007; Cai et al., 2015). The Mongolian Altai (including Gobi Altai) contains an immense volume of granitic intrusions (Fig. 1) and is generally a vital portion of the CAOB (e.g., Şengör et al., 1993; Windley et al., 2007). Recent zircon U–Pb age results demonstrate that these granitic intrusions were mainly emplaced in the Devonian and lesser in Late Carboniferous–Permian and Triassic (e.g., Kozakov et al., 2007; Jiang et al., 2012; Cai et al., 2015; Soejono et al., 2016; Dash et al., 2016). The whole-rock Sm–Nd and zircon Hf isotopic studies indicate that the Devonian granitoids mainly derived from newly formed juvenile crustal materials (Kozakov et al., 2007; Jiang et al., 2012; Soejono et al., 2016; Cai et al., 2015), Late Carboniferous–Permian granitoids would be related to man-

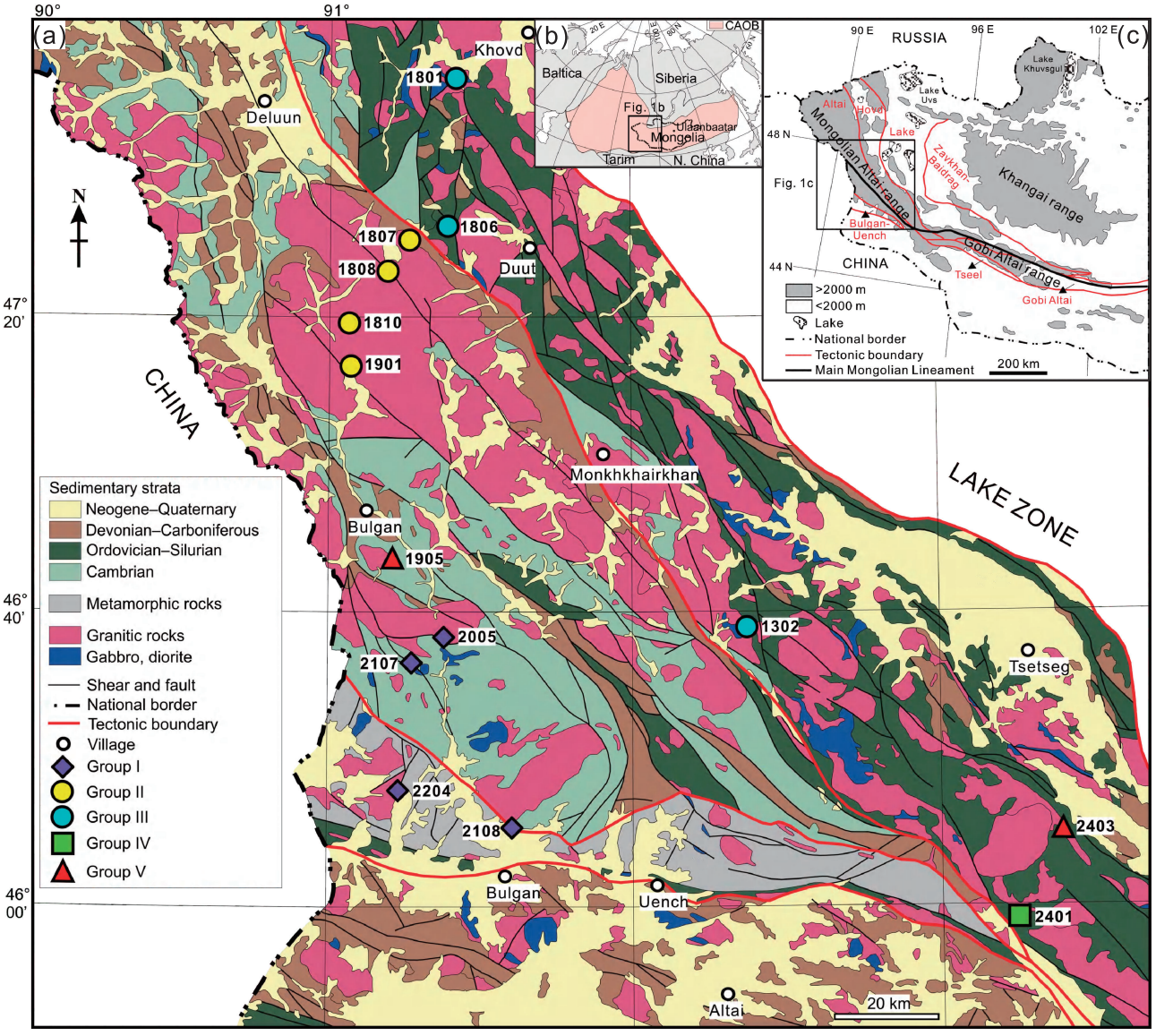

Figure 1. Distribution map of granitic rocks in the Mongolian Altai modified from the 1:500 000 geological map of Mongolia (Erdenechimeg et al., 2017). (a) Sample locations and analysed rock types (group I–V). (b) Location of Mongolia is illustrated in the inset map and its surrounding areas (Şengör et al., 1993). (c) A simplified topographic map of western Mongolia with tectonic units modified after (Badarch et al., 2002).

tle-derived magma and/or short-lived crustal materials (Cai et al., 2015; Kozakov et al., 2007), and Triassic granitoids were possibly generated by reworking of short-lived Neoproterozoic-Paleozoic crust (Kozakov et al., 2007; Cai et al., 2015; Dash et al., 2016). These studies focused mostly on the timing of magmatism and its crustal growth rather than magma evolution. However, magma evolution at most periods in the prolonged growth of the Mongolia Altai in the CAOB remains poorly constrained. In this contribution, we present petrography, geochemical composition, and zircon U-Pb geochronology of the Mongolian Altai granitoids to reveal the timing of the magmatism, sources, and their petrogenetic evolution. Our results indicate that granitoids can be grouped into five petrological groups and four geochronological stages, providing new information to understand the crustal formation and evolution of the Mongolian Altai. Minerals abbreviations used in this paper were defined after the work of Whitney and Evans (2010).

GEOLOGICAL BACKGROUND

The SW Mongolian geological structure covers two major domains affected by Early Paleozoic and Late Paleozoic tectonic events (e.g., Badarch et al., 2002; Windley et al., 2007; Lehmann et al., 2010; Kröner et al., 2010 and references therein). These domains are separated by a crustal-scale fault zone, the Main Mongolian Lineament, which forms an approximate regional structural boundary (e.g., Badarch et al., 2002). In agreement with previous tectonic models, the Mongolian Altai and Gobi Altai are localized in the margin of the Early Paleozoic northern domain. This study investigated the granitic rocks exposed in the Mongolian Altai region (Fig. 1) situated in the boundary zone of the Early Paleozoic to Late Paleozoic domains. The Mongolian Altai region comprises mainly Early Cambrian to Early Devonian sedimentary sequences with a huge amount of granitic rocks (Fig. 1a; Soejono et al., 2017; Long et al., 2020). The sedimentary sequences are composed of a thick sequence (over 4000 m) mainly comprising arkosic sandstone and slate, and those rocks experienced variable deformation and metamorphism and chemically immature, compositionally similar to graywacke (e.g., Long et al., 2020, and reference therein). The host metasedimentary sequences commonly show NW-SE to WNW-ESE-trending strike with dips W to S structures. The metamorphic age of low-grade micaschist and paragneisses are ~ 455, ~ 435, and ~ 385 Ma from in-situ Th-U-Pb monazite grains (Soejono et al., 2021). The greenschist to amphibolite facies metamorphic rocks in this area distribute in a narrow zone that trends WNW-ESE, extending for more than 600 km from Bulgan, Uench in the Mongolian Altai to Tseel in the Gobi Altai, and farther to the southeast (Fig. 1c). This metamorphic belt comprises a layered sequence of pelitic gneisses, amphibolite, and schists locally intruded by granitoids. Two main clusters of metamorphic ages were recognized from those metamorphic rocks: Late Devonian to Early Carboniferous and Permian (e.g., Kozakov et al., 2002, 2011, 2019; Jiang et al., 2012; Burenjargal et al., 2014; Broussolle et al., 2015; Nakano et al., 2014, 2015, 2021b). Granitic intrusions crop out in many places in the Mongolian Altai have predominant emplacement ages of 420-350 Ma with a subordinate age population in the range of 320-260 Ma and 240-210 Ma (e.g., Kozakov et al., 2007; Jiang et al., 2012; Cai et al., 2015; Soejono et al., 2016; Dash et al., 2016). The Gobi Altai including the Tseel area is dominated by low-grade metasedimentary rocks and greenschist to amphibolite facies metamorphic rocks (e.g., Badarch et al., 2002). The protolith age of Gobi Altai was recognized 580-450 Ma by detrital zircon from low-grade siltstone, high-grade paragneisses, pelitic gneisses, and metapelites (Kröner et al., 2010; Jiang et al., 2012; Burenjargal et al., 2014; Nakano et al., 2021b), and these protoliths were metamorphosed together with Mongolia Altai at Late Devonian to Early Carboniferous and Permian (e.g., Kozakov et al., 2002, 2011, 2019; Jiang et al., 2012; Burenjargal et al., 2014; Broussolle et al., 2015; Nakano et al., 2014, 2015, 2021b). The Gobi Altai hosted three generations of magmatic rocks of Middle Devonian to Early Carboniferous (385-345 Ma), Middle to Late Carboniferous (335-307 Ma), and Early Permian (290-271 Ma) ages (Kozakov et al., 2007; Hrdličková et al., 2008; Demoux et al., 2009; Jiang et al., 2012; Cai et al., 2014; Buriánek et al., 2016; Hanžl et al., 2016; Burenjargal et al., 2014; 2016).

PETROGRAPHY

Our study investigates granitic rocks from the Mongolian Altai that can be classified into five groups (Fig. 1a). The mineral assemblages are shown in Table 1.

Group-I includes Bt-Ms granite (2204A, 2005A, and 2005B), Ms-Tur granite (2107), and leucogranite (2108) with massive structure. They were intruded into metamorphic rocks and can be regarded as post-tectonic structures (Figs. 2a and 2b). The main constituents of the former two rock types are Ms, Kfs, Pl, and Qz with or without Bt and Tur (Fig. 3a). The leucogranite consists of Kfs, Pl, Qz, and a minor amount of Bt.

Group-II includes coarse-grained Crd-Bt granite (1901A, 1807A, and 1810; Figs. 2c and 2d) and Bt granite (1808). The Crd-Bt granite is massive and contains euhedral Crd, Bt, Pl, Kfs, and Qz with or without Grt

Table 1. Mineral assemblages of the analyzed samples from the Mongolian Altai

Sample No.	Rock name	Major minerals										Accessory mineral						Secondary mineral
		Pl	Qz	Kfs	Hbl	Bt	Ms	Grt	Crd	Tur	Ep	Ttn	Ap	Zrn	Aln	Mnz	Opq	
Group I																		
2204A	Bt–Ms granite	○	○	○		△	+						+	+			+	
2005A	Bt–Ms granite	△	○	○		△	+						+	+			+	
2005B	Bt–Ms granite	○	○	○		△	+						+	+				
2107	Ms–Tur granite	△	○	○			+			△				+				Chl
2108	Leucogranite	○	○	○		+							+	+		+	+	Chl
Group II																		
1901A	Crd–Bt granite	○	○	○		△		+	+				+	+				Ms
1807A	Crd–Bt granite	△	○	○		+			+				+	+				Ms
1810A	Crd–Bt granite	△	○	○		△			+				+	+				Sericite
1808	Bt granite	△	○	○		△								+				Ms
Group III																		
1302A	Hbl–Bt diorite	○	+		△	○							+	+			+	
1806A	Hbl–Bt granite	○	○	○	△	△						+	+	+	+		+	
1806B	MME hosted in Hbl–Bt granite	○	△	+	○	○						+	+	+			+	
1801A	Bt granite	○	△	○		△						+	+	+		+	+	Ms, Cal
1801B	MME in Bt granite	○	△	+	△	○						+	+	+			+	
Group IV																		
2401A	Bt quartz syenite	+	△	○		+	+	+			+			+	+		+	Chl
2401B	Bt quartz syenite	+	△	○		+		+			+	+		+	+		+	
Group V																		
1905A	Kfs-porphyritic Bt granite	△	○	○		△							+	+		+	+	Ep, Ms
2403A	Kfs-porphyritic Bt granite	△	○	○		△						+	+	+			+	Ms

○, high modal abundance (>20%); △, moderate modal abundance (>10 and ≤20%); +, low modal abundance (≤10%).
Pl, plagioclase; Qz, quartz; Kfs, K-feldspar; Hbl, hornblende; Bt, biotite; Ms, muscovite; Grt, garnet; Crd, cordierite; Tur, tourmaline; Ep, epidote; Ttn, titanite; Ap, apatite; Zrn, zircon; Aln, allanite; Mnz, monazite; Opq, opaque; Cal, calcite; Chl, chlorite.

(Fig. 3b). Nearly all the cordierite has euhedral shape and is inclusion-poor; although some enclose small euhedral Bt flakes, grain size is similar to Pl, Bt, and Qz. The Bt granite consists of Bt, Kfs, Qz, Pl, lack of Crd and Grt. Note that group-II Bt granite can be easily distinguished from group-I Bt granite by its coarse-grained texture.

Group-III includes medium-grained Hbl-Bt granite (1806A) and Bt granite (1801A), which contain mafic magmatic enclave (MME; Figs. 2e and 2f). They have massive structure and hypidiomorphic texture without any deformation (Figs. 2e and 2f). The main constituents are Bt, Pl, Qz with or without Hbl, and Kfs (Fig. 3c). The MME (1806B and 1801B) is fine-grained and Pl-porphyritic texture with a similar mineral assemblage but different in model composition compared to host granite (Fig. 3d). Hbl-Bt diorite (1302A) has similar petrographic features to MME of group-III; therefore, this rock is also included in this group.

Group-IV and -V are Bt quartz syenite (2401A, B; Fig. 2g) and Kfs-porphyritic Bt granite (1905A, 2403A; Figs. 2h and 2j), respectively. The former comprises Kfs, Qz, and minor amounts of Pl, Bt, Ep, Grt, and Ms (Fig. 3e). The latter shows euhedral porphyritic texture with Kfs phenocrysts, and the matrix is mainly Bt, Pl, and Qz (Fig. 3f).

WHOLE-ROCK GEOCHEMICAL FEATURES

All analyses were performed using instruments housed at Kyushu University, Japan. Whole-rock major and trace elements were analyzed using the RIGAKU Primus II X-ray fluorescence (XRF) spectrometer with fused glass disks (2:1 sample dilution). Before fusion, all samples were heated at 880 °C for 2.5 h to remove volatiles and to oxidize ferrous iron. The concentrations of rare earth elements (REEs) and five trace elements (Hf, Ta, Pb, Th, and U) were determined by laser ablation-inductively coupled plasma-mass spectrometry (LA-ICP-MS) using an Agilent 7500cx quadrupole ICP-MS with a New Wave Research UP-213 laser. The analytical procedure was described by Nakano et al. (2012), and the results are attached in Supplementary Table S1 and Figure S1 (Table S1 and Fig. S1 are available online from https://doi.org/

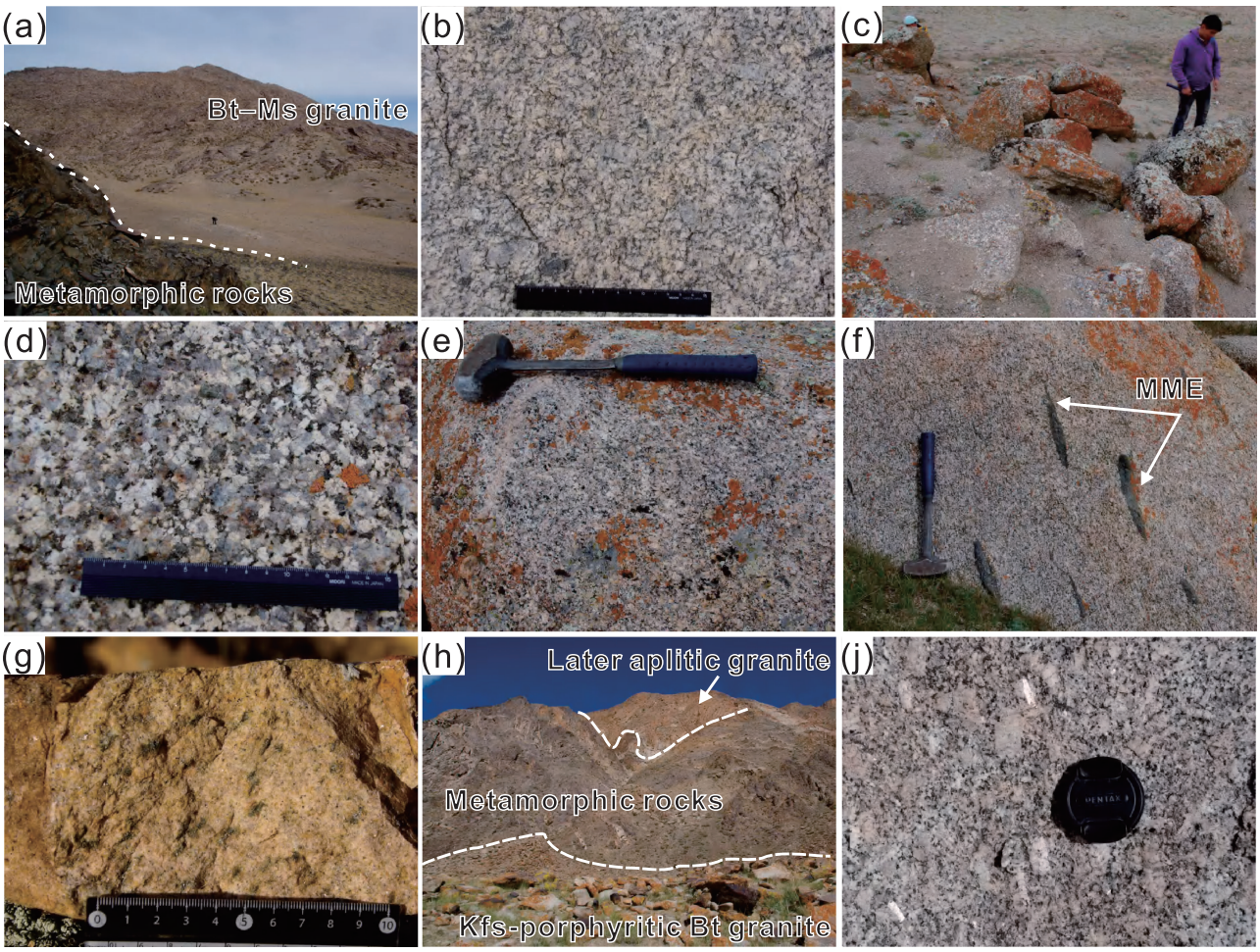

Figure 2. Mode of occurrences for representative samples in each group. (a) and (b) Bt-Ms granite (sample 2204A) intruded into metamorphic rocks in group-I. (c) and (d) Crd-Bt granite (sample 1901A) in group-II. (e) and (f) Hbl-Bt granite (sample 1806A) contains mafic magmatic enclave (MME, sample 1806B) in group-III. (g) Bt quartz syenite (sample 2401A) in group-IV. (h)-(j) Kfs-porphyritic Bt granite (sample 1905A) intruded into metamorphic rocks in group-V.

10.2465/jmps.210830).

Group-I granite has high-SiO_2 content (70-77 wt%) and high total alkalis (K_2O + Na_2O) contents of 7.5-8.6 wt% (Fig. 4a), plotting in the granite field on the total alkali-silica (TAS) diagram (Fig. 4a). These samples are having high-K_2O contents, indicating high-K calc-alkaline and are weakly peraluminous affinity with alumina saturation index [ASI; molar ratio of $Al_2O_3/(CaO + Na_2O + K_2O)$] values of 0.97-1.11 (Fig. 4b and Fig. S1). On the other hand, they have relatively low-Al_2O_3 (12.1-14.2 wt%), total Fe_2O_3 (0.8-3.4 wt%), and MgO (0.1-1.0 wt%) contents (Table S1). They are slightly enriched in LREE [$(La/Yb)_N$ = 4.59-7.56; $_N$ refers to values normalized to chondrite] with strong negative Eu anomalies (Eu/Eu* = 0.22-0.54). The PM-normalized patterns (Fig. 4d) have positive Rb, Th, U, Pb, negative Nb, and strong negative Ba, Sr, P, Eu, and Ti anomalies, similar to the continental crust affinity. In addition, on the Ta versus Yb diagram (Pearce et al., 1984), they are plotted near the boundary field of syn-collisional and within-plate granite fields (Fig. 6a). They have high-Th/Nb ratio of 1.05-1.15, low-Ba/Th ratio of 2.47-26.48 (Fig. 6d), high-Rb/Sr of 0.52-4.94, and high-Rb/Ba of 1.29-6.40 (Table S1).

Group-II granite has high-SiO_2 (70-75 wt%) and high total alkalis ranging from 6.4 to 8 wt% (Fig. 4a). They also have high-K_2O content and high-ASI values (1.04-1.16; Fig. 4b and Fig. S1), indicating high-K calc-alkaline peraluminous affinity. They have relatively low-Al_2O_3 (11.9-13.8 wt%), total Fe_2O_3 (2.2-4.0 wt%), and MgO (0.4-1.3 wt%) contents (Table S1). They are slightly enriched in LREE [$(La/Yb)_N$ = 3.58-5.70] with strong negative Eu anomalies (Eu/Eu* = 0.26-0.47). The PM-normalized patterns (Fig. 4f) have positive Rb, Th, U, Pb, negative Nb, and strong negative Ba, Sr, P, Eu, and Ti anomalies. Most of samples from group-II are plotted near the boundary between volcanic arc granite fields

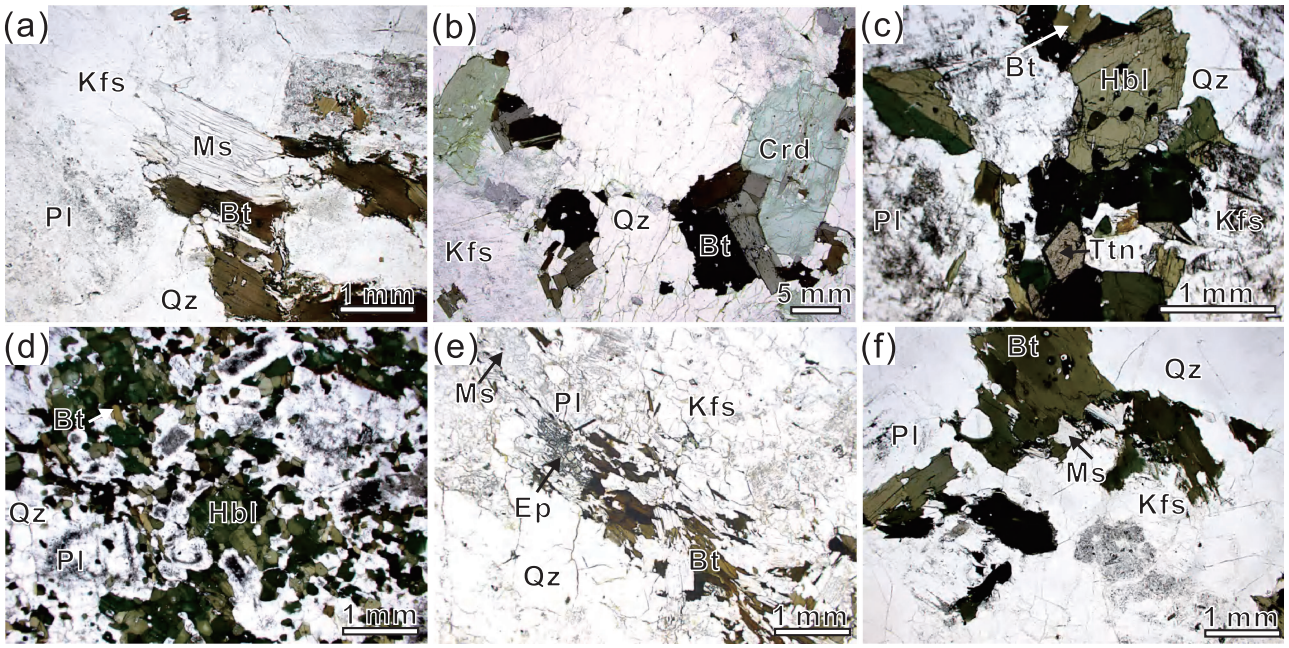

Figure 3. Photomicrographs of representative samples in each group. (a) Bt-Ms granite (sample 2204A). (b) Crd-Bt granite (sample 1901A). (c) Hbl-Bt granite (sample 1806A). (d) mafic magmatic enclave (MME, sample 1806B) hosted in Hbl-Bt granite. (e) Bt quartz syenite (sample 2401A). (f) Kfs-porphyritic Bt granite (sample 1905A).

(Fig. 6a; Pearce et al., 1984). They have high-Th/Nb ratio of 0.90-1.68, low-Ba/Th ratio of 10.91-47.52 (Fig. 6d), high-Rb/Sr of 0.92-7.31, and high-Rb/Ba of 0.25-2.88 (Fig. 6e and Table S1). We note that the chemical features of group-II granite are similar to group-I granite.

Group-III granite, diorite, and related MME have relatively low-SiO_2 (52-69 wt%), and total alkalis are ranging from 4.9 to 7.3 wt%, plotting diorite- to granite fields (Fig. 4a). These samples are medium- to high-K calc-alkaline and are metaluminous affinity with low-ASI values (0.80-0.97; Figs. 4a, 4b and Fig. S1). They have high-Al_2O_3 (14.8-17.8 wt%), total Fe_2O_3 (3.1-10.3 wt%) and MgO (0.8-4.6 wt%) contents (Table S1). They display moderate enrichment of LREE [$(La/Yb)_N$ = 3.54-13.00] and flat-HREE patterns with variable Eu anomalies (Eu/Eu* = 0.57-1.21; Figs. 4c and 4g). In the primitive mantle (PM)-normalized trace element patterns (Fig. 4f), they are enriched in Ba and Sr but depleted in Rb, Th, U, Pb, Nb, Ta, Ti, and HREE. Moreover, on the Ta versus Yb diagram (Pearce et al., 1984), they are plotted in volcanic arc granite fields (Fig. 6a). They have low-Th/Nb ratio of 0.06-0.50, high-Ba/Th ratio of 101-454 (Fig. 6d), low-Rb/Sr of 0.05-0.36, and low-Rb/Ba of 0.05-0.14 (Fig. 6e and Table S1).

Group-IV quartz syenite is a silicate-oversaturated rock and has SiO_2 contents of 66-68 wt%. They are characterized by extremely high total alkalis (11.8-12.0 wt%), defined as alkaline and shoshonitic affinity (Fig. 4a). They have low-MgO (<0.1 wt%) and moderate-Al_2O_3 (15.8-16.5 wt%) contents (Table S1). They display variable LREE-highly enriched and HREE-flat patterns with $(La/Yb)_N$ ratios of 25-33 and strong negative Eu anomalies (Eu/Eu* = 0.22-0.23; Figs. 4c and 4i). Quartz syenite is enriched in LILE with weakly negative Nb and Ta anomalies, negative Sr, P, and Ti anomalies, and positive Pb anomalies and distinct from the oceanic island basalt (OIB) and typical continental crust (Sun and McDonough, 1989; Taylor and McLennan, 1995) (Fig. 4h). They have Th/Nb ratio of 0.51-0.57, Ba/Th ratio of 7.38-9.07, Rb/Sr of 4.22-4.77, and Rb/Ba of 0.94-1.05 (Table S1).

Group-V granite has SiO_2 content of 68 wt% and total alkalis ranging from 8.18 to 9.21 wt%, suggesting

Figure 4. Granitoid classification diagrams. (a) TAS diagram (after Middlemost, 1994) and the alkaline and subalkaline division (after Peccerillo and Taylor, 1976). (b) Plot of ASI $(Al_2O_3/CaO + Na_2O + K_2O)_{molar}$ versus A/NK $(Al_2O_3/Na_2O + K_2O)_{molar}$ (after Maniar and Piccoli, 1989). (c) Plot of Eu/Eu* versus $(La/Yb)_N$, where $Eu/Eu^* = Eu_N/\sqrt{[(Sm_N) \times (Gd_N)]}$, and $_N$ indicates C1 chondrite normalization; normalizing value from is from Sun and McDonough (1989). (d)-(i) Primitive mantle-normalized trace elements pattern and Chondrite-normalized REE patterns. The data for oceanic island basalt (OIB) and normalizing values are from Sun and McDonough (1989). The lower crust, upper crust, and continental crust data are from Taylor and Mclennan (1995).

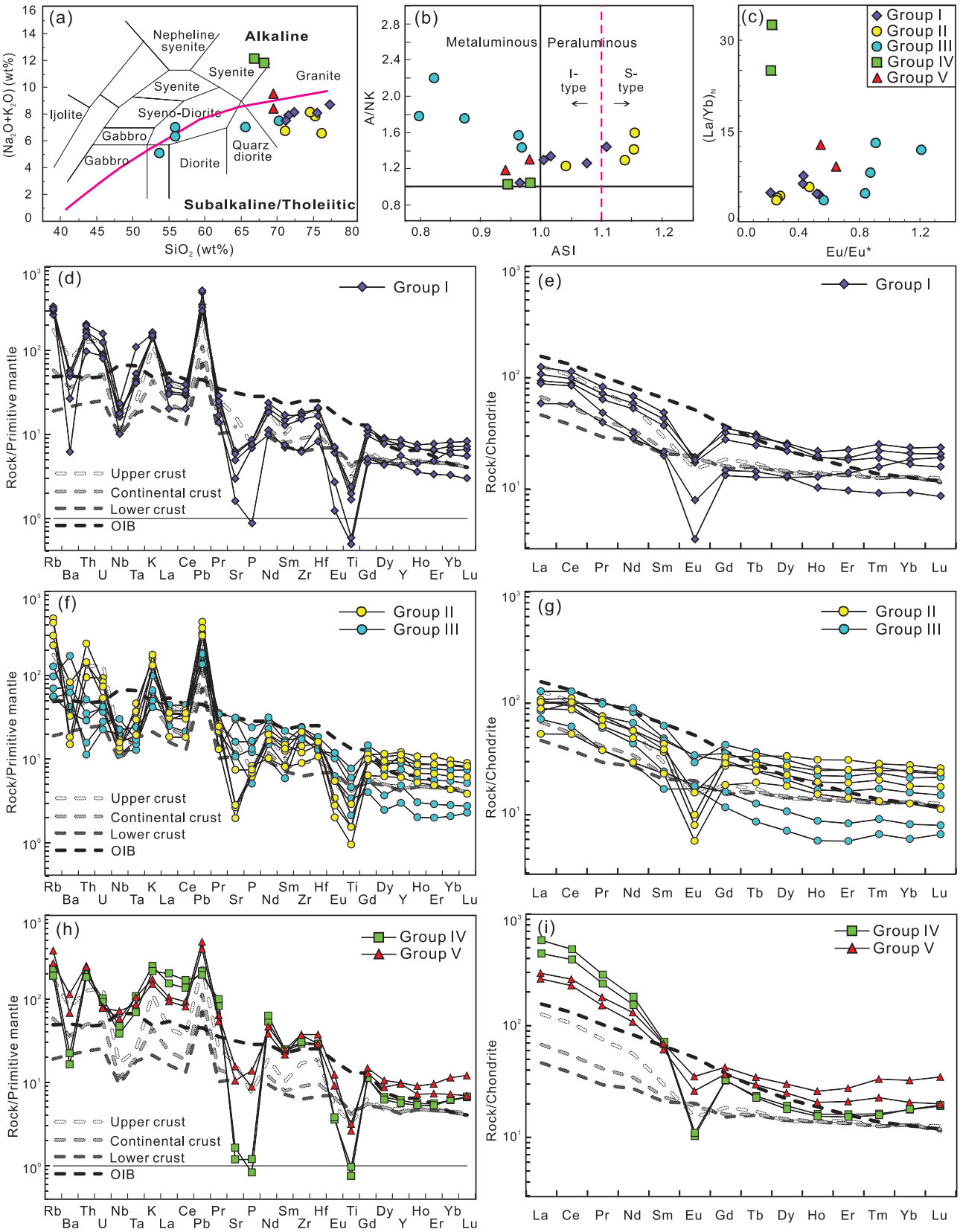
(a)
Nepheline syenite
Alkaline
Syenite
Granite
Syenite
Ijolite
Syeno-Diorite
Gabbro
Quarz diorite
Gabbro
Diorite
Subalkaline/Tholeiitic
(Na2O+K2O) (wt%)
SiO2 (wt%)
(b)
Metaluminous
Peraluminous
I-type
S-type
A/NK
ASI
(c)
Group I
Group II
Group III
Group IV
Group V
(La/Yb)N
Eu/Eu*
(d)
Group I
Upper crust
Continental crust
Lower crust
OIB
Rock/Primitive mantle
Rb Ba Th U Nb Ta K La Ce Pb Pr Sr P Nd Sm Zr Hf Eu Ti Gd Dy Y Ho Er Yb Lu
(e)
Group I
Rock/Chondrite
La Ce Pr Nd Sm Eu Gd Tb Dy Ho Er Tm Yb Lu
(f)
Group II
Group III
Upper crust
Continental crust
Lower crust
OIB
Rock/Primitive mantle
(g)
Group II
Group III
Rock/Chondrite
(h)
Group IV
Group V
Upper crust
Continental crust
Lower crust
OIB
Rock/Primitive mantle
(i)
Group IV
Group V
Rock/Chondrite

high-K calc-alkaline to shoshonitic affinities (Fig. 4a). The low-ASI values (0.94-0.98) indicate a metaluminous feature (Fig. 4b). They have moderate-Al_2O_3 (14.1-14.5 wt%), total Fe_2O_3 (2.8-3.7 wt%), and MgO (0.8-1.0 wt%) contents (Table S1). They show moderately enriched LREE and relatively flat-middle REE to heavy REE patterns with $(La/Yb)_N$ ratios of 9.11-12.77 and negative Eu anomalies (Eu/Eu* = 0.55-0.65; Fig. 4c). The PM-normalized patterns display positive anomalies in Rb, Th, K, Pb, Nb, Ta, and negative anomalies in Ba, Sr, P, Eu, and Ti (Fig. 4h). The samples are plotted in within-plate granite fields (Fig. 6a; Pearce et al., 1984). They have low-Th/Nb ratio of 0.40-0.51, low-Ba/Th ratio of 23.26-37.79, Rb/Sr of 0.51-1.06, and Rb/Ba of 0.21-0.50 (Table S1).

ZIRCON U-Pb AGE DATING

Zrn crystals from the above-described samples were separated and mounted in an epoxy disc with a 25 mm diameter and 4 mm thickness, following separation from powdered samples by panning with a beaker and watch glass, then handpicking (Kitano et al., 2014). After that, the internal structures and inclusions of the individual zircon grains were imaged using a scanning electron microscope (JEOL JSM-6390A) with a cathodoluminescence (CL) detector (Gatan MiniCL). These images were then used as guides of each analytical spot. Zircon U-Pb age dating was performed using LA-ICP-MS of Agilent 7500cx quadrupole ICP-MS coupled with a Photon Machines Analyte G2 193 nm Excimer laser at Kyushu University. The isotopes ^{202}Hg, ^{204}Pb, ^{206}Pb, ^{207}Pb, ^{208}Pb, ^{232}Th, and ^{238}U were monitored throughout the analyses, which were carried out using laser spot size of 20-25 μm. The zircon reference standards Temora (417 Ma; Black et al., 2003) and 91500 (Wiedenbeck et al., 1995) were used for calibration and FC-1 (1099 Ma; Paces and Miller, 1993) to determine the precision, respectively. In addition, a NIST SRM-611 glass standard was used to determine the Th/U ratios. The analytical procedure is described in detail in Nakano et al. (2021a). Concordia diagrams and weighted mean $^{206}Pb/^{238}U$ ages were determined using Isoplot/Ex 3.7 software (Ludwig, 2008). GLITTER software (Griffin et al., 2008) was used to calculate isotopic ratios and dates. All age uncertainties are reported at the 2σ confidence level, and more than 3% of discordant data were omitted from the age calculations. FC-1 standard analyses yielded a concordia age of 1100 ± 3 Ma (95% confidence intervals; n = 61; MSWD = 1.04) in this study. The results are listed in Supplementary Table S2, and the obtained ages are summarized in Table 2. The CL images of analyzed Zrn, concordia diagrams for representative samples, are shown in Figure 5.

The zircon grains from the analyzed granitic rocks are euhedral- to subhedral crystal, prismatic, and elongated in shape with the aspect ratio of 1-3. In addition, zircon shows oscillatory zoning (Figs. 5a-5f) with high Th/U ratios (Table S2), indicating a magmatic origin.

Group-I: The Zrn grains from Bt-Ms granite (2204A) gave a weighted mean $^{206}Pb/^{238}U$ age of 375 ± 4 Ma (n = 16, Th/U = 0.27; Fig. 5a) from the Zrn rim, whereas inherited core gave ages of 943-420 Ma (Fig. 5a). The Zrn grains from Bt-Ms granite (2005A) show a weighted mean $^{206}Pb/^{238}U$ age of 381 ± 13 Ma (n = 9, Th/U = 0.37) from the rim, while the ages from the core vary between 1210 and 450 Ma. The Zrn grains from Ms-Tur granite (2107) gave a concordia age of 387 ± 4 Ma (n = 10, Th/U = 0.21) from the rims, and a single analysis of a core gives an age of 440 Ma. The leucogranite (2108) contains Zrn grains, yielding a concordia age of 361 ± 4 Ma (n = 9, Th/U = 0.62) from the rim, and a single analysis of a core gives an age of 400 Ma.

Group-II: The Zrn from Crd-Bt granite (1901A) yielded a concordia age of 369 ± 5 Ma (n = 10, Th/U = 0.23; Fig. 5b) from the Zrn rim, whereas Zrn cores have 460-410 Ma ages as inherited ages. Zrn grains from Bt granite (1808) show a weighted mean $^{206}Pb/^{238}U$ age of 353 ± 5 Ma (n = 9, Th/U = 0.38).

Group-III: The Zrn grains from Hbl-Bt granite (1806A), yielded a concordia age of 366 ± 3 Ma (n = 13, Th/U = 0.50; Fig. 5c). The Zrn from MME (1806B) yielded a weighted mean $^{206}Pb/^{238}U$ age of 356 ± 6 Ma (n = 9, Th/U = 0.65; Fig. 5d), which is almost identical within the analytical error to the crystallization age (366 ± 3 Ma) of host Hbl-Bt granite (Fig. 5c).

Group-IV: Zrn grains from Bt quartz syenite (2401A) shows a homogeneous dark-CL wide core with a very narrow bright-CL rim (Fig. 5e). The bright-CL rim is too narrow to be analyzed. However, we detected two age clusters from the dark-CL wide core during the measurement. The rim portion of the dark-CL core gave a concordia age of 315 ± 6 Ma (n = 5, Th/U = 0.52), while the center portion of the dark-CL core gave 370-350 Ma (Fig. 5e).

Group-V: The Zrn grains from Kfs-porphyritic Bt granite (1905A) yielded a concordia age of 208 ± 1 Ma (n = 24, Th/U = 0.57), while analyzed cores gave older discordant ages (Fig. 5f). The Zrn grains from Kfs-porphyritic Bt granite (2403A) yielded a concordia age of 200 ± 1 Ma (n = 22, Th/U = 0.83).

DISCUSSION

Timing of magmatism in the Mongolian Altai

Zircon U-Pb ages, geochemical characteristics, and pet-

Table 2. Summary of the LA-ICP-MS zircon U-Pb ages of granitic rocks from the Mongolian Altai

Sample No.	Rock name	Coordinates		Magmatic age (Ma)	Inherited age (Ma)
		N latitude	E longitude		
Group I					
2204A	Bt–Ms granite	46°12'06"	91°12'01"	375 ± 4 (n = 16, MSWD = 1.9) Th/U =0.27	440–420, 940 (n = 5)
2005A	Bt–Ms granite	46°34'22"	91°24'00"	381 ± 13 (n = 9, MSWD = 0.58) Th/U =0.37	1210, 1150, 450 (n = 3)
2107	Ms–Tur granite	46°28'07"	91°14'41"	387 ± 4 (n = 10, MSWD = 1.8) Th/U =0.21	440 (n = 1)
2108	Leucogranite	46°05'59"	91°32'52"	361 ± 4 (n = 9, MSWD = 0.08) Th/U =0.62	400 (n = 1)
Group II					
1901A	Crd–Bt granite	47°10'55"	91°05'23"	369 ± 5 (n = 10, MSWD = 2.6) Th/U =0.23	460–410 (n = 7)
1808	Bt granite	47°24'38"	91°13'22"	353 ± 5 (n = 9, MSWD = 1.7) Th/U =0.38	
Group III					
1806A	Hbl–Bt granite	47°30'38"	91°26'01"	366 ± 3 (n = 13, MSWD = 1.2) Th/U =0.50	
1806B	Mafic magmatic enclave	47°30'38"	91°26'01"	356 ± 6 (n = 9, MSWD = 2.0) Th/U =0.65	
Group IV					
2401A	Bt quartz syenite	45°55'13"	93°12'54"	315 ± 6 (n = 5, MSWD = 1.6) Th/U =0.52	370–350 (n = 7)
Group V					
1905A	Kfs-porphyritic Bt granite	46°40'09"	91°21'33"	208 ± 1 (n = 24, MSWD = 0.9) Th/U =0.57	
2403A	Kfs-porphyritic Bt granite	46°11'16"	93°21'12"	200 ± 1 (n = 22, MSWD = 0.55) Th/U =0.83	

rological investigations of the granitic rocks in the Mongolian Altai reveal four stages of magmatic activity: (1) 387–361 Ma group-I granite, (2) 369–353 Ma includes groups-II and -III granites, (3) ~ 315 Ma group-IV quartz syenite, and (4) 208–200 Ma group-V granite, as discussed in detail below.

Stage (1): zircon U-Pb age results of granites from group-I gives zircon U-Pb age of 387–361 Ma as a magmatic age. Stage (2): zircon U-Pb age result of groups-II and -III granites constrain that those two group granites were contemporaneously emplaced at 369–353 and 366–356 Ma. These ages are also in line with zircon ages of 390–380 Ma for high-grade metamorphism of the granulite and amphibolite facies (Bibikova et al., 1992; Kozakov et al., 2002, 2011, 2019; Jiang et al., 2012) and 370–356 Ma for relatively low-grade metamorphism of the amphibolite facies (Kozakov et al., 2002, 2011, 2019; Burenjargal et al., 2014; Broussolle et al., 2015; Nakano et al., 2014) from the Mongolian Altai and Gobi Altai. Moreover, recent zircon U-Pb age dating results of igneous rocks demonstrate that Devonian magmatism was widespread in the Mongolia Altai and Gobi Altai regions (e.g., Kozakov et al., 2007; Kröner et al., 2010; Jiang et al., 2012; Cai et al., 2015; Burenjargal et al., 2016; Soejono et al., 2016; Hanžl et al., 2016; Buriánek et al., 2016). Stage (3): we interpret the age of 315 Ma from the Zrn core as an emplacement age of group-IV quartz syenite. In addition, Late Carboniferous magmatism mainly affected the boundary between the Early Paleozoic northern and Late Paleozoic southern domains. Stage (4): the geochronological result of group-V granite gives zircon U-Pb age of 208–200 Ma as the timing of emplacement. Their emplacement was separated by long periods from the main magmatic activity in the Mongolian Altai.

Petrogenesis of the Mongolian Altai granitoids

Group-I (387-361 Ma) granites. Group I granite contain Bt and Ms except for leucogranite and has weakly peraluminous feature with ASI values of 0.97–1.11, indicating they have peraluminous affinity (Chappell et al., 2012). Group-I granite displays positive Rb, Th, U, and Pb with

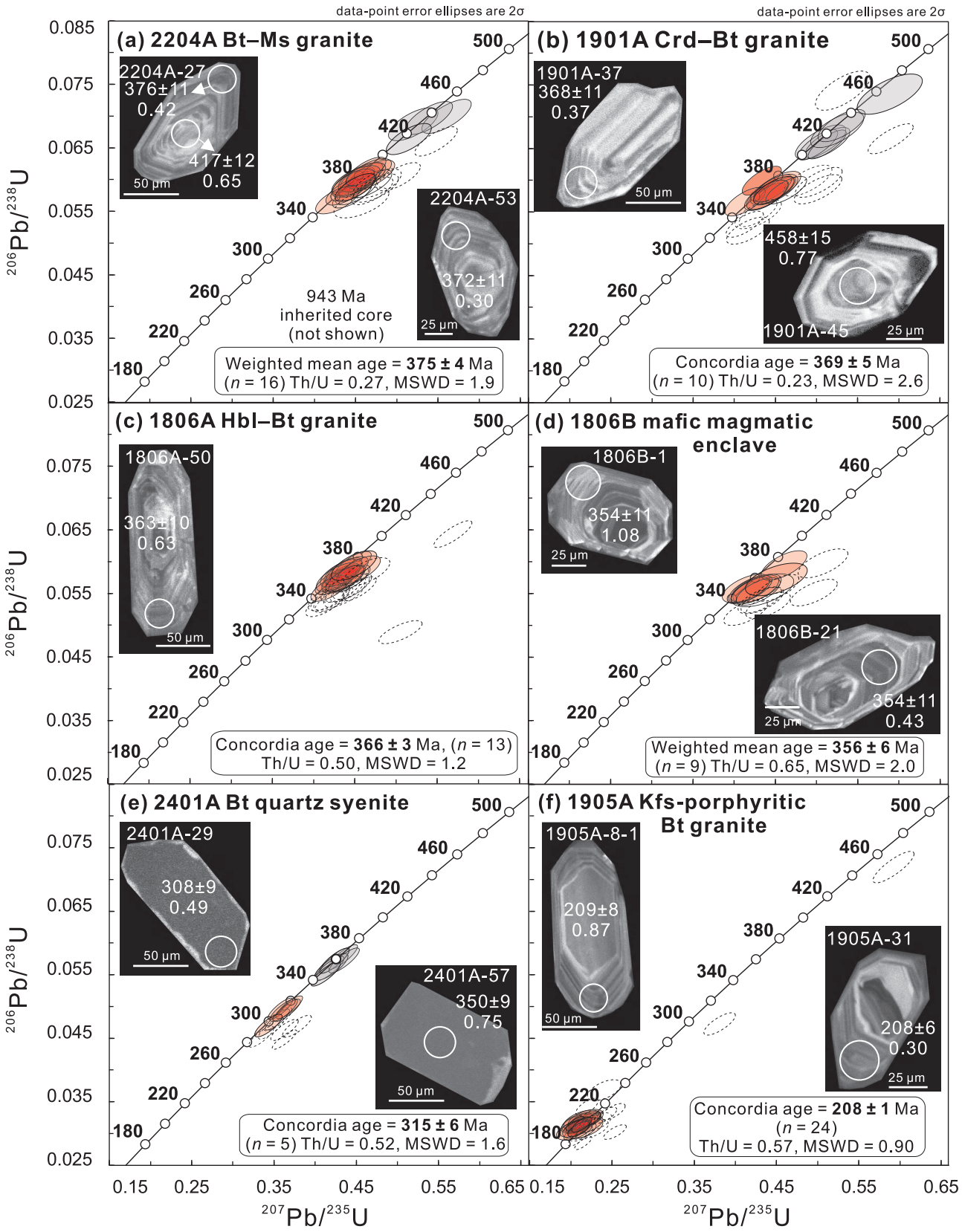

Figure 5. Concordia diagrams, cathodoluminescence (CL) images with analysis spots, apparent $^{206}Pb/^{238}U$ spot ages (upper numbers) and Th/U ratios (lower numbers) for representative analyzed samples from the Mongolian Altai. The concordant and discordant data are shown as solid and dashed ellipses, respectively. Grey color-filled ellipses indicate inherited Zrn, and red color-filled ellipses indicate magmatic Zrn.

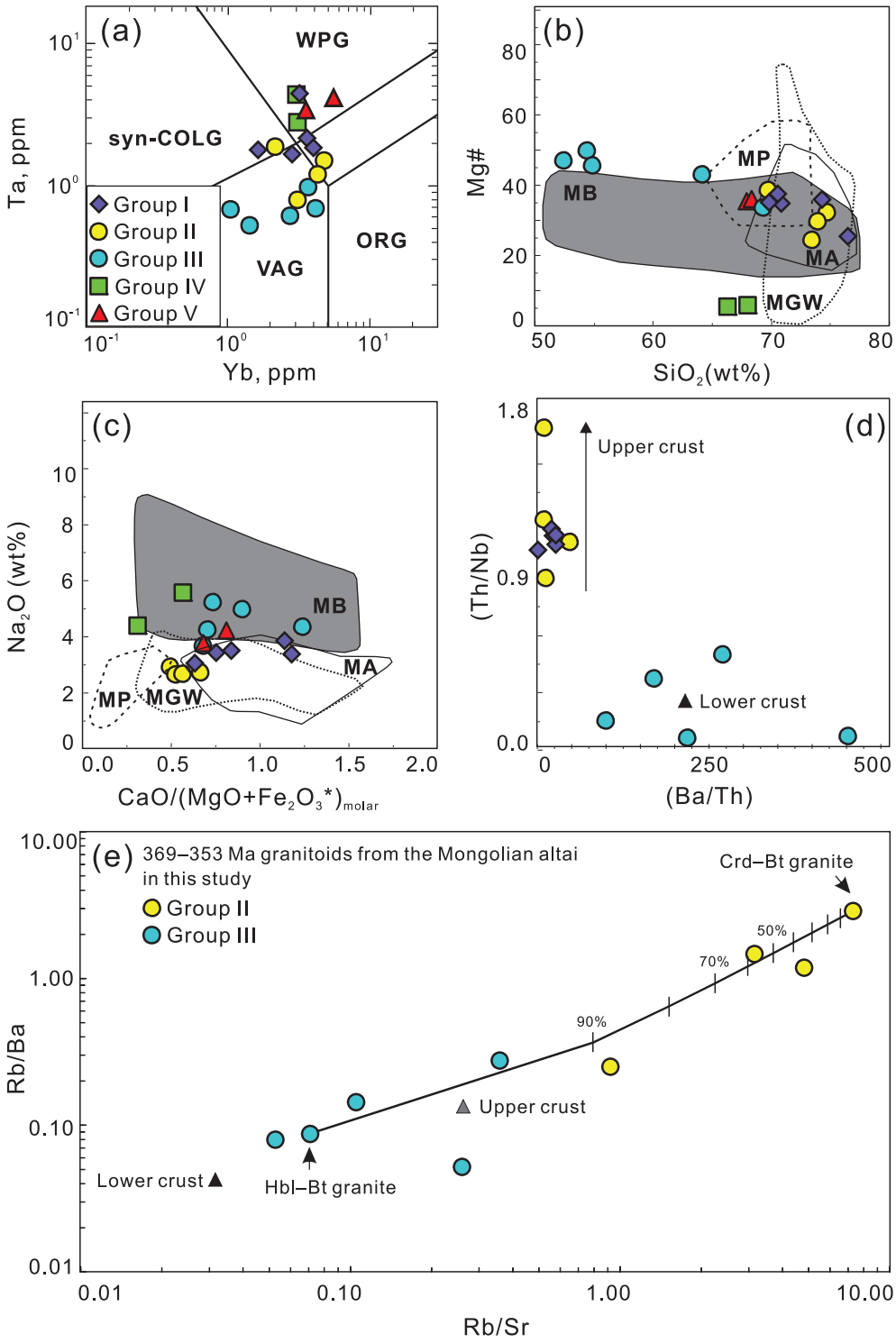

Figure 6. Granitoid discrimination diagrams. (a) Ta versus Yb discrimination diagram for granitic rocks. Fields of volcanic arc granites (VAG), syn-collisional granites (syn-COLG), within-plate granites (WPG), and ocean-ridge granites (ORG) are after Pearce et al. (1984). (b) and (c) Source discrimination diagrams for granitic rocks from the Mongolian Altai. Outlined fields denote compositions of partial melts obtained in experimental studies by dehydration melting of various bulk compositions. MB, metabasalts (shaded); MA, meta-andesites (solid line); MGW, metagreywakes (dotted line); MP, metapelites (dashed line). Data sources: Altherr and Siebel (2002) and reference therein. (d) Ba/Th versus Th/Nb diagram with trends for upper crust and lower crust. Lower crust value from Taylor and Mclennan (1995). (e) Rb/Ba versus Rb/Sr diagram for group-II and -III granites from the Mongolian Altai with the binary mixing curve between the Hbl-Bt granite (1801A) and Crd-Bt granite (1807A) in this study. Lower and upper crust values from Taylor and Mclennan (1995).

negative Nb, strong negative Ba, Sr, P, and Ti anomalies in PM-normalized trace element patterns, and negative Eu anomaly with enriched-LREE to flat-HREE chondrite-normalized patterns (Figs. 4d and 4e), indicating continental crust signature (Taylor and McLennan, 1995). Unlike many trace elements, whose interpretation in granitic systems is complicated by the presence of accessory mineral phases, practically all of the Rb, Sr, and Ba in granitic systems is contained in mica and feldspar (e.g., Harris and Inger, 1992; Sylvester, 1998). Therefore, those elements mainly play a role in their origin. Moreover, the behavior of trace element ratio such as Th/Nb can be used as tracers of sediment contribution in the source of magma because Th is enriched in sediments and incompatible in the melt (Brenan et al., 1995; Johnson and Plank, 1999). In the discrimination diagram relating to source, group-I granite is pointing towards an origin by dehydration melting of meta-andesites and/or metagreywackes (Figs. 6b and 6c). However, they have high-Rb/Sr of 0.52-4.94 and high-Rb/Ba of 1.29-6.40 ratios, with respect to magmas generated by partial melting of metagreywackes (Sylvester, 1998). Group-I granite has high-Th/Nb and low-Ba/Th ratios (Fig. 6d), suggesting that magma source was mainly derived from sedimentary rocks, which is further supported by the presence of inherited Zrn. Therefore, our result suggests group-I peraluminous granite in the Mongolian Altai was possibly formed by partial melting of mainly immature sediments like metagreywackes that would leave behind large amounts of plagioclase (Montel and Vielzeuf, 1997). Because Sr and Ba are compatible in plagioclase, whereas Rb is incompatible (Harris and Inger, 1992), melts derived from such sources will tend to have higher Rb/Sr and Rb/Ba ratios than their sources (Sylvester, 1998). This is one of the possible causes for the negative Eu anomalies of group-I granite (Fig. 4e) due to the plagioclase being the main carrier of Eu. In the Mongolian Altai, the sedimentary sequence is mainly composed of a thick sequence (4000-6000 m) of slate, phyllitic shale, mica schist, and greywacke (Long et al., 2020, reference therein), which contains abundant hydrous minerals, e.g., Bt and Ms. We suggest that these hydrous minerals break down incongruently at middle crust level and supply water and felsic components to a melt phase (Patiño Douce, 1999).

Group-II (369-353 Ma) granites. Group-II granites contain euhedral Crd and Bt, and all samples have peraluminous feature with high-ASI values of 1.04-1.16, suggesting they are peraluminous granite (Chappell and White, 2001). In comparison, group-I and -II granites display similar behavior in PM-normalized trace element patterns and chondrite-normalized REE patterns, where they show positive Rb, Th, U, and Pb with negative Nb, strong negative Ba, Sr, P, Eu, and Ti anomalies (Figs. 4d-4g), indicating continental crust signature (Taylor and McLennan, 1995). For the magma source discrimination diagram, Figures 6b and 6c imply dehydration melting of immature metagreywackes for the origin of group-II granite. It is supported by their high-Th/Nb and low-Ba/Th ratios (Fig. 6d) and inherited Zrn.

Group-III (366-356 Ma) granites. In contrast, the group-III granite and associated mafic magmatic enclave are classified as diorite to granite fields (Fig. 4a) and a medium- to high-K calc-alkaline series. Meanwhile, most group-III granitoids contain Hbl, have metaluminous features with low ASI values of 0.80-0.97, and are suggested to be metaluminous granite (Chappell and White, 2001). They also show enrichment in Ba and Sr and depletion in Rb, Th, U, Pb, Nb, Ta, and Ti in the PM-normalized patterns (Fig. 4d) and comparable to continental crust (Taylor and McLennan, 1995). Other geochemical features like the low-Sr/Y (4.42-19.26) <20 and low-La/Yb (4.93-18.12) <20 ratios suggest the group-III granites do not have adakitic geochemical affinity (e.g., Moyen, 2009). One sample (1801A) has a high Sr concentration of 620 ppm and a positive Eu anomaly of 1.21, indicating plagioclase accumulation. The partial melting of the crust largely involves dehydration melting processes play an essential role in the granitic magma generation (e.g., Chappell et al., 2012). In the discrimination diagrams relating to source, the group-III granitoids are compatible with an origin by dehydration melting from the metabasaltic source (Figs. 6b and 6c; Rapp and Watson, 1995). The low-Th/Nb and high-Ba/Th ratios of group-III granitoids are comparable with mafic lower crustal material from Taylor and McLennan, 1995 (Fig. 6d). Also, they have low-Rb/Sr and low-Rb/Ba ratios, and it is chemically comparable with partial melts predominantly derived from the gabbroic lower crustal material (Fig. 6e). Furthermore, group-II peraluminous and group-III metaluminous granites were formed contemporaneously, and their Rb/Ba versus Rb/Sr correlation (Fig. 6e) define a linear trend, indicating a two-component mixing process. Hence, it suggests that group-III metaluminous magma would carry heat to the crust, inducing partial melting of sedimentary rocks to produce group-II peraluminous granite, then mixing in the source of these two components in proportions. Moreover, group-III granite from NE portion possibly to be lower-sequence and group-II granite from SW portion possibly to be upper-sequence, regarding their NW-SE to WNW-ESE, strike with dips W to S structures (Fig. 1). Therefore, we assume that group-II peraluminous granite in the Mongolian Altai was possibly formed by partial melting of metagreywackes as immature sediments. However, the lack of isotopic data from group-II

granites needs further study. Nevertheless, previous studies reported whole-rock $\varepsilon_{Nd}(t)$ values from −2.1 to +5.7 with Nd model ages between 0.95–0.60 Ga and Zrn $\varepsilon_{Hf}(t)$ values from +0.5 to +19.2 with Hf model ages between 1.02–0.31 Ga from the Devonian granitoids in the Mongolian Altai (Kozakov et al., 2007; Cai et al., 2015). Based on the isotopic data, they concluded that the Devonian granitoids were mainly derived from newly formed juvenile crustal materials buried in the deep crust, with the addition of mantle-derived mafic magma. Our whole-rock chemical data of group-III granite has reached a similar conclusion. We note that different textural and chemical features between the Devonian granitoids in the Mongolian Altai are probably due to different source rocks involved in the melting and cooling environments.

Group-IV (~ 315 Ma) quartz syenite. The group-IV quartz syenite is exposed in the boundary between the Mongolian Altai and Gobi Altai. Since the sampling of quartz syenite was limited, a detailed discussion of petrogenetic processes is difficult. Instead, this study documented quartz syenites have SiO_2 contents of 66–68 wt% and low-MgO (<0.1 wt%) with shoshonitic affinity and distinct geochemical features of those continental crust that they are strongly depleted in Sr, Eu, P, and Ti, enriched in Nb, Ta, and LREE (Figs. 4a, 4h, and 4i). Moreover, the presence of inherited Zrn indicates crustal assimilation during magma evolution. However, numerous petrological, geochemical, and experimental studies have suggested that the lithospheric mantle and crust are possible sources for syenites (e.g., Huang and Wyllie, 1975; Litvinosky and Steele, 2000; Laporte et al., 2014). Moreover, syenitic magmas appear to be polygenetic, and it is generally assumed that syenite magma characterizes anorogenic, within-plate environments. The age of quartz syenite is ~ 315 Ma, which is in line with the dating of Cai et al. (2015) from the same area, indicates that the crustal extension occurred after main orogenic magmatism (387–353 Ma) and mainly affected the boundary between the Early Paleozoic northern domain and Late Paleozoic southern domain. We suppose that quartz syenite might have a genetic link to Sagsai alkali-gabbroic and quartz monzonite pluton in the Gobi Altai, evidenced by coeval emplacement age of 322–307 Ma (Buriánek et al., 2016). The positive Zrn $\varepsilon_{Hf}(t)$ values of +7.4 to +11.5 from Sagsai alkali-gabbroic pluton suggested depleted mantle-derived magma source, and Sagsai alkali-gabbroic and quartz monzonite pluton were formed in post-subduction extensional regime proposed by Buriánek et al. (2016). Our geochemical and geochronological data of quartz syenite support this idea that group IV quartz syenite would be derived from depleted mantle-derived magma source accompanied by crustal assimilation during magma evolution.

Group-V (208–200 Ma) granites. Kfs-porphyritic granite has high-K calc-alkaline to shoshonitic affinities with low-ASI values of 0.94–0.98, suggesting metaluminous granite. Accordingly, group-V granite intrusions contain euhedral Kfs phenocryst and lack of deformation features, and intruding into high- and low-grade metamorphic rocks in the Mongolian Altai are evidences for considering them being post-orogenic granites.

CONCLUDING REMARKS

Newly investigated petrological, geochemical, and zircon U-Pb geochronological studies of the Mongolian Altai granitoids lead to the following conclusions:

1) Group-I (Bt-Ms granite) and -II (Crd-Bt granite) have high-K calc-alkaline and peraluminous affinity, whereas group-III (Hbl-Bt granite) has calc-alkaline and metaluminous affinity. Group-IV (Bt quartz syenite) and -V (Kfs-porphyritic granite) show shoshonitic- to high-K calc-alkaline and metaluminous affinity.
2) Groups-I, -II, and -III have continental crust-like multi-elements and REEs patterns, whereas groups-IV and -V have different patterns with strongly depleted in Sr, P, and Ti, enriched in Nb, Ta, and LREE.
3) Group-I granite yields 387–361 Ma, whereas group-II and -III granites yield 369–353 and 366–356 Ma as magmatic ages, respectively. Group-IV quartz syenite and group-V granite yield ~ 315 and 208–200 Ma as emplacement ages.
4) Groups-I and -II peraluminous granites have high-Th/Nb, and low-Ba/Th reflecting sources might be derived from sedimentary rocks, whereas group-III metaluminous granite has low-Th/Nb, and high-Ba/Th reflecting source might be derived from gabbroic crustal material.
5) Groups-I and -II peraluminous granites have similar geochemical characteristics, but their emplacement ages are different, which suggests they were formed from different magmas.
6) Group-II peraluminous and group III metaluminous granites were contemporaneously formed at 369–353 Ma. Their Rb/Ba versus Rb/Sr correlation define a linear trend of the magma mixing process. It demonstrates that group-III metaluminous magma would carry heat to the crust, inducing partial melting of sedimentary rocks to produce group-II peraluminous granite.
7) Geochemical and geochronological data of groups-I, -II, and -III granites demonstrate that they were

formed during the main orogenic activity in the Mongolian Altai, which is also consistent with the timing of the main metamorphic event at Late Devonian to Early Carboniferous. Subordinate occurrences of group-IV quartz syenite and group-V granite were probably formed in extensional to post-collisional environments after main orogenic activity in the Mongolian Altai.

ACKNOWLEDGMENTS

We thank D. Khashbat, Ts. Bolormaa, Ch. Boldbaatar, P. Choidogjamts and G.Tsogbayar for their help during the field expeditions in the Mongolian Altai. We are deeply indebted to M. Satish-Kumar for his comments and editorial handling, and three anonymous reviewers for their critical and constructive comments. This study was funded from a Project for Human Resources Development Scholarship of Japanese Grant Aid (JDS) at Kyushu University and supported by JSPS KAKENHI Grant Numbers JP21253008, JP22244063, and JP16H02743 to Y. Osanai; JP15K05345, JP18H01316, and 21K18381 to N. Nakano.

SUPPLEMENTARY MATERIALS

Supplementary Figure S1, Supplementary Table S1, and Supplementary Table S2 are available online from https://doi.org/10.2465/jmps.210830.

REFERENCES

Altherr, R. and Siebel, W. (2002) I-type plutonism in a continental back-arc setting: Miocene granitoids and monzonites from the central Aegean Sea, Greece. Contributions to Mineralogy and Petrology, 143, 397-415.

Arndt, N.T. (2013) Formation and evolution of the continental crust. Geochemical Perspectives, 2, 405-433.

Badarch, G., Cunningham, W.D. and Windley, B.F. (2002) A new terrane subdivision for Mongolia: implications for the Phanerozoic crustal growth of Central Asia. Journal of Asian Earth Sciences, 21, 87-110.

Barbarin, B. (1999) A review of the relationships between granitoid types, their origins and their geodynamic environments. Lithos. 46, 605-626.

Bibikova, E.V., Kirnozova, T.I. and Kozakov, I.K. (1992) Polymetamorphic complexes of the Southern Slone of the Mongolia and Gobi Altai: result of U-Pb dating. Geotektonika, 2, 104-112.

Black, L.P., Kamo, S.L., Allen, C.M., Aleinikoff, J.N., et al. (2003) TEMORA 1: a new zircon standard for Phanerozoic U-Pb geochronology. Chemical Geology, 200, 155-170.

Brenan, J.M., Shaw, H.F., Ryerson, F.J. and Phinney, D.L. (1995) Mineral-aqueous fluid partitioning of trace elements at 900 °C and 2.0 GPa: constraints on the trace element chemistry of mantle and deep crustal fluids. Geochimica et Cosmochimica Acta, 59, 3331-3350.

Broussolle, A., Štípská, P., Lehmann, J., Schulmann, K., et al. (2015) P-T-t-D record of crustal-scale horizontal flow and magma-assisted doming in the SW Mongolian Altai. Journal of Metamorphic Geology, 33, 359-383.

Burenjargal, U., Okamoto, A., Kuwatani, T., Sakata, S., et al. (2014) Thermal evolution of the Tseel terrane, SW Mongolia and its relation to granitoid intrusions in the Central Asian Orogenic Belt. Journal of Metamorphic Geology, 32, 765-790.

Burenjargal, U., Okamoto, A., Tsuchiya, N., Uno, M., et al. (2016) Contrasting geochemical signatures of Devonian and Permian granitoids from the Tseel Terrane, SW Mongolia. Journal of Geosciences, 61, 51-66.

Buriánek, D., Janoušek, V., Hanžl, P., Jiang, Y., et al. (2016) Petrogenesis of the Late Carboniferous Sagsai Pluton in the SE Mongolian Altai. Journal of Geosciences, 61, 67-92.

Cai, K.D., Sun, M., Xiao, W.J., Yuan, C., et al. (2014) Petrogenesis of late Paleozoic tholeiite, calc-alkaline and adakitic rocks in the southwestern Mongolia: implications for intraoceanic arc evolution. Lithos, 202-203, 413-428.

Cai, K., Sun, M., Jahn, B., Xiao, W., et al. (2015) A synthesis of zircon U-Pb ages and Hf isotopic compositions of granitoids from Southwest Mongolia: Implications for crustal nature and tectonic evolution of the Altai Superterrane. Lithos, 232, 131-142.

Chappell, B.W. and White, A.J.R. (2001) Two contrasting granite types: 25 years later. Australian Journal of Earth Sciences, 48, 489-499.

Chappell, B.W., Bryant, C.J. and Wyborn, D. (2012) Peraluminous I-type granites. Lithos, 153, 142-153.

Dash, B., Boldbaatar, E., Zorigtkhuu, O. and Yin, A. (2016) Geochronology, geochemistry and tectonic implications of Late Triassic granites in the Mongolian Altai Mountains. Journal of Asian Earth Sciences, 117, 225-241.

Demoux, A., Kröner, A., Hegner, E. and Badarch, G. (2009) Devonian arc-related magmatism in the Tseel terrane of SW Mongolia: chronological and geochemical evidence. Journal of the Geological Society, London, 166, 459-471.

Erdenechimeg, D., Tomurtogoo, O., Boldbaatar, G., Enkhbayar, B., et al. (2017) Geological map of Mongolia 1: 500000, Geo Information data-2013 project, report No. 8480, appendix 14-17, Geological Investigation Center, Ulaanbaatar, Mongolia (in Mongolian).

Griffin, W.L., Powell, W.J., Pearson, N.J. and O'Reilly, S.Y. (2008) GLITTER: Data reduction software for laser ablation ICP-MS. Mineralogical Association of Canada Short Course, 40, 308-311.

Hanžl, P., Schulmann, K., Janoušek, V., Lexa, O., et al., (2016) Making continental crust: origin of Devonian orthogneisses from SE Mongolian Altai. Journal of Geosciences, 61, 25-50.

Harris, N.B.W. and Inger, S. (1992) Trace element modelling of pelite-derived granites. Contributions to Mineralogy and Petrology, 110, 46-56.

Hrdličková, K., Bolormaa, Kh, Buriánek, D., Hanžl, P., et al., (2008) Petrology and age of metamorphosed rocks in tectonic slices inside the Palaeozoic sediments of the eastern Mongolian Altay, SW Mongolia. Journal of Geosciences, 53, 139-165.

Huang, W.L. and Wyllie, P.J. (1975) Melting reaction in the system $NaAlSi_3O_8$-$KalSi_3O_8$-SiO_2 to 35 kilobars, dry and with excess water. The Journal of Geology, 83, 737-748.

Jahn, B.M., Wu, F. and Chen, B. (2000) Massive granitoid generation in Central Asia: Nd isotope evidence and implication for continental growth in the Phanerozoic. Episodes, 23, 82-92.

Jiang, Y., Sun, M., Kröner, A., Tumurkhuu, D., et al. (2012) The high-grade Tseel Terrane in SW Mongolia: An Early Paleozoic arc system or a Precambrian silver? Lithos, 142-143, 95-115.

Johnson, M.C. and Plank, T. (1999) Dehydration and melting experiments constrain the fate of subducted sediments. Geochemistry Geophysics Geosystems, 1, 1007.

Kitano, I., Osanai, Y., Nakano, N., Adachi, T., et al. (2014) Rapid techniques for zircon separation and the application for U-Pb dating. Bulletin of the Graduate School Social and Culture Studies, Kyushu University, 20, 1-10 (in Japanese with English abstract).

Kozakov, I.K., Glebovitsky, V.A., Bibikova, E.V., Azimov, P.Y., et al. (2002) Hercynian granulites of Mongolian and Gobian Altai: geodynamic setting and formation conditions. Doklady Earth Sciences, 386, 781-785.

Kozakov, I.K., Kovach, V.P., Bibikova, E.V., Kirnozova, T.I., et al. (2007) Age and sources of granitoids in the junction zone of the Caledonides and Hercynides in southwestern Mongolia: geodynamic implications. Petrology, 15, 126-150.

Kozakov, I.K., Didenko, A.N., Azimov, P.Ya., Kirnozova, T.I., et al. (2011) Geodynamic Settings and Formation Conditions of Crystalline Complexes in the South Altai and South Gobi Metamorphic Belts. Geotectonics, 45, 174-194.

Kozakov, I.K., Kozlovsky, A.M., Yarmolyuk, V.V., Kirnozova, T.I., et al. (2019) Geodynamic Environments of the Origin of Poly- and Monometamorphic Complexes in the Southern Altai Metamorphic Belt, Central Asian Orogenic Belt. Petrology, 27, 223-242.

Kröner, A., Lehmann, J., Schulmann, K., Demoux, A., et al. (2010) Lithostratigraphic and geochronological constraints on the evolution of the Central Asian Orogenic Belt in SW Mongolia: early Paleozoic rifting followed by late Paleozoic accretion. American Journal of Science, 310, 523-574.

Laporte, D., Lambart, S., Schiano, P. and Ottolini, L. (2014) Experimental derivation of nepheline syenite and phonolite liquids by partial melting of upper mantle peridotites. Earth and Planetary Science Letters, 404, 319-331.

Lehmann, J., Schulmann, K., Lexa, O., Corsini, M., et al. (2010) Structural constraints on the evolution of the Central Asian Orogenic Belt in SW Mongolia. American Journal of Science, 310, 575-628.

Litvinosky, B.A. and Steele, I.M. (2000) Silicic magma formation in overthickened crust: melting of charnockite and leucogranite at 15, 20 and 25 kbar. Journal of Petrology, 41, 717-737.

Long, X., Luo, J., Sun, M. and Wang, X. (2020) Detrital zircon U-Pb ages and whole-rock geochemistry of early Paleozoic metasedimentary rocks in the Mongolian Altai: Insights into the tectonic affinity of the whole Altai-Mongolian terrane. The Geological Society of America Bulletin, 132, 477-494.

Ludwig, K.R. (2008) User's Manual for Isoplot 3.70: a geochronological toolkit for Microsoft Excel. Berkeley Geochronology Center Special Publication 4.

Maniar, P.D. and Piccoli, P.M. (1989) Tectonic discrimination of granitoids. Geological Society of America Bulletin, 101, 635-643.

Middlemost, E.A.K. (1994) Naming materials in the magma/igneous rock system. Earth-Sciences Reviews, 37, 215-224.

Montel, J.M. and Vielzeuf, D. (1997) Partial melting of metagreywackes: Part II. Compositions of minerals and melts. Contributions to Mineralogy and Petrology, 128, 176-196.

Moyen, J.F. (2009) High Sr/Y and La/Yb ratios: the meaning of the "adakitic signature." Lithos, 112, 556-574.

Nakano, N., Osanai, Y., Adachi, T., Yonemura, K., et al. (2012) Rapid techniques for quantitative determination of major, trace and rare earth elements in low dilution glass bead using XRF and LA-ICP-MS. Bulletin of the Graduate school of Social and Culture Studies, Kyushu University, 18, 81-94 (in Japanese with English abstract).

Nakano, N., Osanai, Y., Satish-Kumar, M., Adachi, T., et al. (2014) Paleozoic subduction-accretion-closure histories in the west Mongolian segment of the Paleo-Asian Ocean: evidence from pressure-temperature-time-protolith evolution of high- Mg and -Al schists in the Altai Mountains. The Journal of Geology, 122, 283-308.

Nakano, N., Osanai, Y., Owada, M., Satish-Kumar, M., et al. (2015) Multiple growth of garnet, sillimanite/kyanite and monazite during amphibolite facies metamorphism: implications for the *P-T-t* and tectonic evolution of the western Altai Range, Mongolia. Journal of Metamorphic Geology, 33, 937-958.

Nakano, N., Osanai, Y., Owada, M., Binh, P., et al. (2021a) Evolution of the Indochina block from its formation to amalgamation with Asia: constraints from protoliths in the Kontum Massif, Vietnam. Gondwana Research, 90, 47-62.

Nakano, N., Osanai, Y., Jargalan, S., Adachi, T., et al. (2021b) Petrology and geochronology of andalusite- and sillimanite-bearing kyanite metapelites from the Gobi Altai Mountains: Evidence for prolonged convergent tectonics in the Central Asian Orogenic Belt. Lithos, 400-401.

Paces, J.B. and Miller, J.D.J. (1993) U-Pb ages of Duluth complex and related mafic intrusions, northeastern Minnesota: geochronological insights to physical, petrogenetic, paleomagnetic, and tectonomagmatic processes associated with thee 1.1 Ga midcontinent rift system. Journal of Geophysical Research, 98, 13997-14013.

Patiño Douce, A.E. (1999) What do experiments tell us about the relative contributions of crust and mantle to the origin of granitic magmas? In Understanding granites: Integrating new and classical techniques (Castro, A., Fernandez, C., Vigneresse, J.L. Eds). Geological Society London Special Publications, 168, 55-75.

Pearce, J.A., Harris, N.B.W. and Tindle, A.G. (1984) Trace element discrimination diagrams for the tectonic interpretation of granitic rocks. Journal of Petrology, 25, 956-983.

Peccerillo, A. and Taylor, S.R. (1976) Geochemistry of Eocene Calc-Alkaline Volcanic rocks from the Kastamonu Area, Northern Turkey. Contributions to Mineralogy and Petrology, 58, 63-81.

Rapp, R.P. and Watson, E.B. (1995) Dehydration melting of metabasalt at 8-32 kbar: implications for continental growth and crust-mantle recycling. Journal of Petrology, 36, 891-931.

Rudnick, R.L. (2003) Composition of the Continental Crust. Treatise on Geochemistry, 3, 1-64.

Şengör, A.M.C., Natal'in, B.A. and Burtman, V.S. (1993) Evolution of the Altaid Tectonic collage and Palaeozoic Crustal Growth in Eurasia. Nature, 364, 299-307.

Soejono, I., Buriánek, D., Svojtka, M., Žáček, V., et al. (2016) Mid-Ordovician and Late Devonian magmatism in the Togtokhinshil Complex: new insight into the formation and accretionary evolution of the Lake Zone (western Mongolia). Jour-

nal of Geosciences, 61, 5–23.
Soejono, I., Buriánek, D., Janoušek, V., Svojtka, M., et al. (2017) A reworked Lake Zone margin: Chronological and geochemical constraints from the Ordovician arc-related basement of the Hovd Zone (western Mongolia). Lithos, 295, 112–132.
Soejono, I., Peřestý, V., Schulmann, K., Čopjaková, R., et al. (2021) Structural, metamorphic and geochronological constraints on Palaeozoic multi-stage geodynamic evolution of the Altai accretionary wedge system (Hovd Zone, western Mongolia). Lithos, 396–397, 1–20.
Sun, S.-S. and McDonough, W.F. (1989) Chemical and isotopic systematics of oceanic basalts: implications for mantle composition and processes. Geological Society, London, Special publications, 42, 313–345.
Sylvester, P.J. (1998) Post-collisional strongly peraluminous granite. Lithos, 45, 29–44.
Taylor, R.S. and McLennan, M.S. (1995) The geochemical evolution of the continental crust. Review of Geophysics, 33, 241–265.
Wiedenbeck, M., Alle, P., Corfu, F., Griffin, W.L., et al. (1995) Three natural zircon standards for U-Th-Pb, Lu-Hf, trace element and REE analyses. Geostandards Newsletter, 19, 1–23.
Windley, B.F., Alexeiev, D., Xiao, W., Kröner, A., et al. (2007) Tectonic models for accretion of the Central Asian Orogenic Belt. Journal of the Geological Society, 164, 31–47.
Whitney, D.L. and Evans, B.W. (2010) Abbreviations for names of rock-forming minerals. American Mineralogist, 95, 185–187.

Manuscript received August 30, 2021
Manuscript accepted January 13, 2022
Published online March 2, 2022
Manuscript handled by M. Satish-Kumar